On Deriving Vertical Air Motions from Cloud Radar Doppler Spectra

MATTHEW D. SHUPE

Cooperative Institute for Research in Environmental Science, and NOAA/Earth System Research Laboratory, Boulder, Colorado

PAVLOS KOLLIAS

Brookhaven National Laboratory, Upton, New York

MICHAEL POELLOT

University of North Dakota, Grand Forks, North Dakota

EDWIN ELORANTA

University of Wisconsin—Madison, Madison, Wisconsin

(Manuscript received 19 March 2007, in final form 12 September 2007)

ABSTRACT

A method for deriving vertical air motions from cloud radar Doppler spectrum measurements is introduced. The method is applicable to cloud volumes containing small particles, in this case liquid droplets, which are assumed to trace vertical air motions because of their limited size. The presence of liquid droplets is confirmed using multiple ground-based remote sensors. Corrections for Doppler spectrum broadening due to turbulence, wind shear, and radar beamwidth are applied. As a result of the turbulence broadening correction, the turbulent dissipation rate can also be estimated. This retrieval is demonstrated using measurements from the Department of Energy (DOE) Atmospheric Radiation Measurement Program's (ARM) site in Barrow, Alaska, during the Mixed-Phase Arctic Cloud Experiment (MPACE) of autumn 2004. Comparisons of the retrievals with measurements by research aircraft near Barrow indicate that, on the whole, the retrievals perform well. A small bias in vertical velocity between the retrievals and aircraft measurements is found, based on a statistical comparison of four cases comprising nearly 6 h of data. Turbulent dissipation rate comparisons suggest that the radar-retrieved vertical velocity might be slightly underestimated because of an underestimate of the turbulence broadening correction. However, large uncertainties in aircraft vertical velocity measurements likely impact the comparison.

1. Introduction

Vertical motions at various scales are integral in cloud formation and persistence processes (e.g., Heymsfield 1975; Paluch and Lenschow 1991; Hogan et al. 2002; Lothon et al. 2005), leading to condensation and evaporation of hydrometeors and impacting the partitioning of water phases within a cloud layer. For example, shallow, weak, small-scale vertical motions play a key role in the life cycle of hydrometeors in stratiform (Paluch and Lenschow 1991; Kollias and Albrecht 2000) and fair-weather cumulus (Kollias et al. 2001) clouds. While the basic physics regarding condensation and evaporation of single cloud particles in response to vertical air motions is understood from a theoretical perspective (e.g., Pruppacher and Klett 1978), the specific role that vertical motions play in shaping the phase composition of clouds is more complex and less understood (Rauber and Tokay 1991). Moreover, a more detailed understanding of the small-scale processes relating vertical motions and cloud properties is necessary to better parameterize cloud formation and maintenance mechanisms within models at many scales. One method to better understand these relations is through the use of long-term observational datasets containing coincident air motion and cloud microphysical properties.

Corresponding author address: Matthew Shupe, R/PSD3, 325 Broadway, Boulder, CO 80305.
E-mail: matthew.shupe@noaa.gov

DOI: 10.1175/2007JTECHA1007.1

Profiling cloud radars measure the vertical motions of cloud particles in the atmosphere. However, both vertical air motions and particle fall speeds contribute to the Doppler velocities measured by cloud radars (e.g., Gossard and Strauch 1983). Moreover, the spectrum of radar Doppler velocities is influenced by turbulence within the radar volume. Thus, the derivation of vertical air motions from vertically oriented cloud radar measurements is only possible under specific sets of conditions. First, with explicit knowledge of the cloud particle size distribution, a quiet-air spectrum of particle fall speeds can be computed that can then be compared to the measured radar Doppler spectrum to provide an estimate of the vertical air motion (e.g., O'Connor et al. 2005). Quiet-air Doppler spectra can also be determined by deconvolving the fall speed and turbulent contributions to the measured radar Doppler spectrum. Such methods rely on assumptions about the shape of the particle size distribution and the particle size–fall speed relationship (Gossard 1994; Gossard et al. 1997) and/or computationally intensive inversion processes (Babb et al. 2000). If only the vertical velocity is desired, a much simpler retrieval can be applied that only requires prior knowledge about the presence of small particles, such as liquid water cloud droplets, in the radar volume that are assumed to be tracers of clear-air motions (e.g., Gossard 1994; Kollias et al. 2001). Here, we exploit this last condition to derive vertical air velocities from cloud radar measurements.

Typical liquid cloud droplets (5–20 μm) have Stokes terminal fall speeds of $\sim$2 cm s^{-1} or less. These fall speeds are negligible with respect to the typical variations of vertical air motions in shallow-convective clouds, which are one–two orders of magnitude larger (Paluch and Lenschow 1991; Kollias and Albrecht 2000; Kollias et al. 2001). Thus, under quiet-air conditions, radar observations of liquid drops should have a Doppler velocity at or very near the 0 m s^{-1} radar velocity bin and a narrow Doppler spectrum width. Under actual conditions, the Doppler spectrum is broader than would be expected from the droplet or particle size distribution alone because of the temporal (signal dwell time) and spatial (radar beamwidth and pulse length) filters that introduce additional broadening due to turbulence and wind shear (e.g., Kollias et al. 2001). Each of these contributions must be understood to derive accurate air motions from Doppler spectra.

In this manuscript, a method is described for retrieving vertical air motions in shallow-convective, stratiform clouds that contain liquid droplets from cloud radar Doppler spectra. The method is demonstrated using a cloud radar in operation at the Department of Energy's Atmospheric Radiation Measurement Program (ARM) Climate Research Facility (ACRF) on the North Slope of Alaska (NSA), located near the coastal town of Barrow, Alaska (71.323°N, 156.616°W). In this case, vertical velocities are derived from observations of Arctic stratiform mixed-phase clouds from the Mixed-Phase Arctic Cloud Experiment (MPACE; Verlinde et al. 2007), which took place in autumn 2004. During this experiment, research aircraft made observations near the NSA site, providing some measurements with which to assess the retrieval method. Although the method is demonstrated here for the case of mixed-phase stratocumulus at an Arctic location, it is presumably applicable to other cloud types observed in other locations as long as small droplets or particles, which trace the vertical air motions, are present. This method is utilized in a companion study that examines the processes that link vertical motions and cloud microphysical properties in Arctic stratiform mixed-phase clouds (Shupe et al. 2008).

TABLE 1. MMCR specifications.

Wavelength	8.7 mm
Beamwidth	0.31°
Dwell time	1 s
Time resolution*	4 s
Range gate length*	45 m
No. of FFTs*	256
Nyquist velocity*	5.27 m s^{-1}
Velocity resolution*	0.041 m s^{-1}

* Specific to the "stratus" mode of operation.

2. Instruments

The focal instrument of this method is the vertically pointing, 35-GHz, Millimeter Cloud Radar (MMCR), which has been the subject of many studies and is thoroughly described elsewhere (Moran et al. 1998; Kollias et al. 2007). Here, only the "stratus" mode is utilized, which has been optimized for observing low-level clouds (see Table 1). The MMCR produces vertically resolved measurements of the Doppler spectrum, which is the distribution of returned radar power as a function of hydrometeor radial (in this case vertical) velocity in the radar volume. The first three moments of the Doppler spectrum—the reflectivity, mean Doppler velocity, and Doppler spectrum variance (and its square root, the "spectrum width")—are commonly used to derive cloud properties. For radar Doppler velocity measurements, the convention is that positive velocities are toward the radar, or down. To maintain consistency, all other measurements and retrievals of air motions follow this same convention.

A number of other instruments from the NSA site support the implementation of this retrieval. A high spectral resolution lidar (HSRL) was deployed at the NSA site during the MPACE time period. This 532-nm system provides profiles of calibrated backscatter and depolarization ratio, which are both crucial for identifying the presence of liquid water, through aerosols and clouds up to an optical depth of ~4, above which the lidar beam is occulted. Brightness temperature measurements at 23.8 and 31.4 GHz from a microwave radiometer (MWR) also provide an estimate of the total condensed liquid water path (LWP; in g m^{-2}), which is used for identifying cloud liquid conditions, based on variable coefficient, bilinear, statistical retrievals (Liljegren et al. 2001; Turner et al. 2007). Measurements of temperature and wind speed are made by periodic radiosonde ascents, with a temporal frequency that varied from four per day during intensive observation periods to typically one per day during standard operations at MPACE. Temperature information is used to support the identification of cloud liquid, while the horizontal winds are useful in the derivation of Doppler spectral broadening terms. Vertically resolved temperature and wind speed profiles are interpolated in time to cover the time periods of interest.

Aircraft in situ measurements near the NSA site are compared with the ground-based retrieval methods. Vertical wind and turbulent dissipation rate estimates are made from aircraft position, speed, and pressure measurements made at the aircraft nose and/or wing and are filtered to remove time periods when icing affected the pressure ports. Turbulence calculations are based on fluctuations in airspeed over distances of ~800 m, assuming isotropy, and have an estimated uncertainty of 0.2 $cm^2 s^{-3}$. The error in vertical air velocities is estimated to be ± 0.5 m s^{-1}.

3. Methods

a. Identifying the presence of cloud liquid

If cloud liquid droplets are present in a radar volume, the retrieval of vertical air motions from radar measurements will be accurate to within the uncertainty of deriving the relatively small bias that is caused by broadening of the Doppler spectrum due to turbulence and wind shear within the radar resolution volume. Therefore, it is imperative to accurately identify the presence of cloud liquid. The cloud phase classification employed here (fully described in Shupe 2007) exploits clear signatures of liquid water from multiple sensors. The case study from 1630 to 1800 UTC 9 October at MPACE will stand as an example for the general classification (Fig. 1) and the subsequent vertical motion retrieval.

Cloud liquid is identified by the high lidar backscatter and low depolarization ratio (e.g., Sassen 1984; Intrieri et al. 2002) that are present near the top of the lidar returns in Figs. 1c,d. High backscatter is due to the high total surface area associated with typical populations of cloud droplets, which are small and exist in relatively high concentrations. Spherical particles, which are typically liquid, do not significantly depolarize the lidar beam, resulting in very small depolarization ratios. On the contrary, nonspherical ice crystals, which are typically larger than liquid droplets and occur in smaller concentrations, highly depolarize the lidar signal and often have less backscatter than water droplets (i.e., below 600 m in Figs. 1c,d). The lidar beam is attenuated by optically thick cloud layers (optical depth > 4), as seen above 800 m. Thus, from lidar alone, there is an indication of cloud liquid occurring above 600 m in the 9 October case, with ice occurring below this level.

The liquid identification by the lidar is supported by retrievals of a positive LWP from MWR measurements (Fig. 1e). In addition, radiosondes indicating water saturation and a temperature inversion (not shown) reveal the presence of liquid water, since a temperature inversion typically occurs near the top of Arctic cloud liquid layers (Pinto 1998; Zuidema et al. 2005). Since radar reflectivity responds to the sixth power of the hydrometer size distribution, the typically larger ice particles in mixed-phase cloud volumes dominate the reflectivity (Fig. 1a). The reflectivity in this case is most often higher than that expected for liquid droplets only (populations of liquid droplets typically do not have a reflectivity larger than -17 dBZ; Frisch et al.1995), indicating that there is cloud ice present above the base of the cloud liquid identified by the lidar. Only near the very top of the radar returns are reflectivities consistent with the presence of small liquid droplets. Together, this combination of measurements can provide a robust identification of cloud liquid, even in the presence of cloud ice.

For the 9 October case, the combined-sensor classification illustrates the basic structure of low-level, stratiform Arctic mixed-phase clouds (Fig. 1f). The cloud region above the lidar cloud base is mostly mixed phase, containing a layer of liquid water from which ice particles form and fall. Below the lidar cloud base (i.e., the cloud liquid base), only ice and snow exist down to the surface. The vertical air motion retrieval can be applied to the cloud regions between the base and the top of the cloud liquid (lines in Fig. 1).

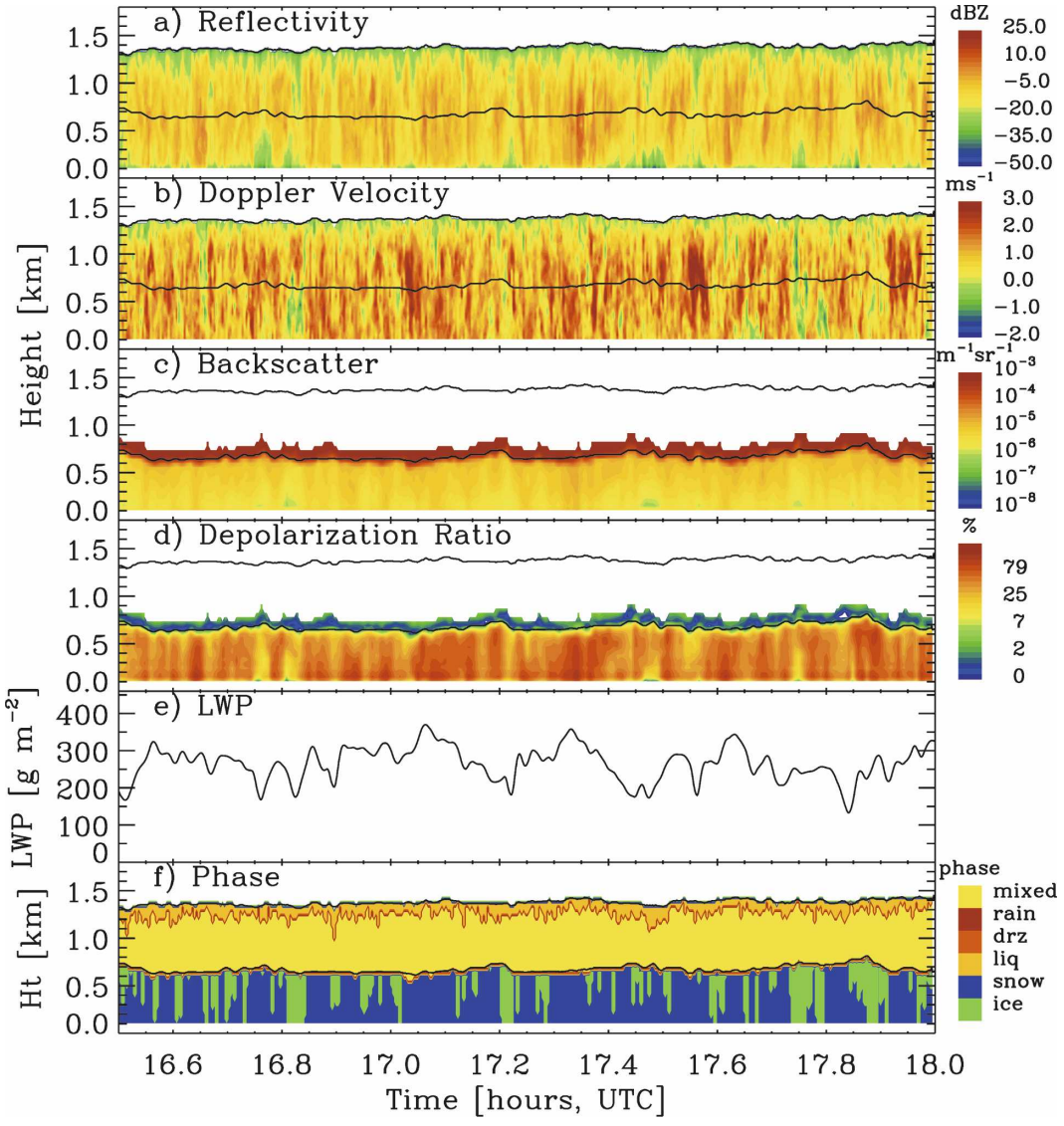

FIG. 1. Measurements on 9 Oct 2004 of (a) radar reflectivity, (b) radar mean Doppler velocity, (c) lidar backscatter, (d) lidar depolarization ratio, (e) microwave radiometer–derived liquid water path, and (f) multisensor-derived cloud phase classification. In most panels, the base and top of the cloud liquid layer, identified from lidar and radar measurements, respectively, are plotted.

b. *Vertical velocity retrieval*

If a radar return is identified to contain liquid water, the vertical velocity, W (m s^{-1} with positive velocities toward the ground), is estimated from the radar Doppler spectrum. First, the spectrum noise is computed using the Hildebrand and Sekhon (1974) technique. If the spectral peak is 30 dB or more above the noise floor, a spectral image due to gain and phase imbalance in the MMCR analog receiver is present. Using the Doppler spectrum postprocessing algorithm described by Kollias et al. (2007), the spectral image and other artifacts (dc component, aliasing) are removed and the main (hydrometeor) spectral peak is identified. Vertical velocities are retrieved using the first spectral peak consisting of at least seven consecutive velocity bins (a width of 0.29 m s^{-1}) above the noise. The liquid cloud droplets occupy the leftmost portion of the spectral peak (smallest fall velocities), and thus, the left spectral edge is identified as the initial vertical air motion estimate prior to the correction for spectral broadening terms (Fig. 2).

The Doppler spectrum variance for a vertically viewing radar is given by

$$\sigma_D^2 = \sigma_{\mathrm{DSD}}^2 + \sigma_T^2 + \sigma_S^2 + \sigma_B^2, \qquad (1)$$

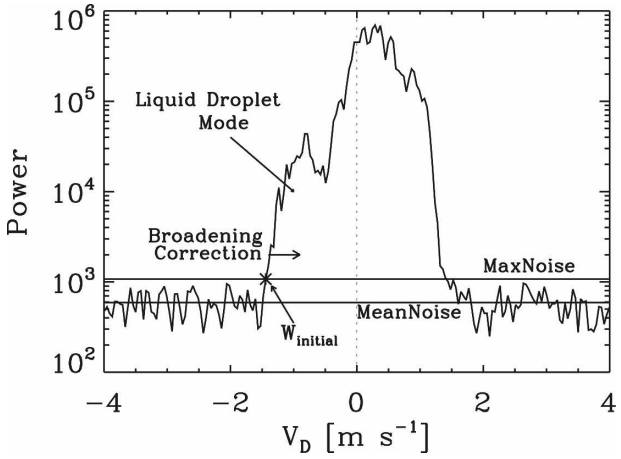

FIG. 2. Measured Doppler spectrum containing spectral modes for both liquid droplets and ice crystals. The mean and maximum noise levels computed via the Hildebrand and Sekhon (1974) method are shown. The initial vertical velocity estimate is indicated by the asterisk, while the location and direction of spectral broadening corrections are indicated by an arrow (although the length of the arrow is much longer than typical corrections).

where $\sigma^2_{\rm DSD}$ is the variance due to the droplet or particle size distribution, σ^2_T is the variance due to turbulence, σ^2_S is the variance due to wind shear, and σ^2_B is the variance due to a finite radar beamwidth; each of these processes is assumed to be independent. To derive vertical air motions from an observed Doppler spectrum, without knowledge of $\sigma^2_{\rm DSD}$, the latter three terms are used to correct for the effects of non–droplet size distribution (DSD) broadening of the left edge of the spectrum.

The contribution to the spectrum variance due to the radar beamwidth, θ (in radians), arises from the variation of horizontal wind contributions to the radial velocity across the beamwidth. This variance is small and, for a circularly symmetric Gaussian antenna pattern, is a function of the horizontal wind speed, U (m s^{-1}), and the radar beamwidth (e.g., Gossard and Strauch 1983):

$$\sigma^2_B = \frac{U^2\theta^2}{2.76}. \tag{2}$$

For a vertically oriented radar with a Gaussian antenna pattern, vertical (k_v) and horizontal (k_h) shear in the vertical winds (both in s^{-1}) causes spectral broadening given by (Gossard and Strauch 1983; Kollias et al. 2001)

$$\sigma^2_S = \frac{k_h^2 R^2\theta^2}{2.76} + \frac{k_v^2\Delta^2}{12}, \tag{3}$$

where the first term describes transverse shear, the second term describes radial (or vertical) shear, R is the range to the pulse volume, and Δ is the range gate length. Here, both terms are based on the shear in the measured mean Doppler velocity across three adjacent points and assume that variation in Doppler velocity on these small scales is not due to changes in particle terminal fall velocities.

Turbulent broadening of the Doppler spectrum is derived from the temporal variance of the measured mean Doppler velocity, $\sigma^2_{\rm vm}$, using a method proposed by Bouniol et al. (2003) and implemented by O'Connor et al. (2005) with a radar similar to the MMCR. The method assumes that the length scales of the turbulent eddies observed by the radar are within the inertial subrange of the turbulence spectrum and that turbulence, rather than fluctuation in particle terminal velocities, is the dominant contribution to $\sigma^2_{\rm vm}$ on the time scales of interest. Bouniol et al. (2003) verified both of these assumptions for a comparable cloud radar observing drizzling stratocumulus clouds, which are similar to the clouds discussed here. The slope of the high-frequency end of the turbulence spectra derived from these measurements (i.e., Fig. 4) is sometimes consistent with the presence of three-dimensional isotropic turbulence, as is found in the inertial subrange (e.g., Curry et al. 1988; Gultepe and Starr 1995), although this is not always the case, suggesting that the inertial subrange may not always be captured. O'Connor et al. (2005) show that both σ^2_T and $\sigma^2_{\rm vm}$ can be described by a similar functional form, namely

$$\sigma^2_T = \int_{k_s}^{k_\lambda} S(k)\,dk = \frac{3a}{2}\left(\frac{\varepsilon}{2\pi}\right)^{2/3}(L_s^{2/3} - L_\lambda^{2/3}) \tag{4}$$

$$\sigma^2_{\rm vm} = \int_{k_l}^{k_s} S(k)\,dk = \frac{3a}{2}\left(\frac{\varepsilon}{2\pi}\right)^{2/3}(L_l^{2/3} - L_s^{2/3}), \tag{5}$$

where the turbulent energy spectrum is $S(k) = a\varepsilon^{2/3}k^{-5/3}$, a is the Kolmogorov constant, ε is the turbulent dissipation rate, k is the wavenumber, and L is the length scale given by $k = 2\pi/L$. In this notation, L_λ is the smallest scale observed by the radar, L_s is the length of the scattering volume for the 1-s dwell time (which includes larger eddies passing through the observed volume), and L_l describes the larger eddies passing through the effective sample volume that results from an average of the radar observations over 60 s. In all cases, the length scales are given as $L = Ut + 2R\sin(\theta/2)$, where t is the observation time. The ratio of (4) and (5) yields the useful relation

$$\frac{\sigma^2_T}{\sigma^2_{\rm vm}} = \frac{L_s^{2/3}}{L_l^{2/3} - L_s^{2/3}}, \tag{6}$$

assuming $L_\lambda^{2/3} \ll L_s^{2/3}$. A secondary product of this system of equations is the turbulent dissipation rate, which can be obtained by rearranging (4) or (5) to yield, for example,

$$\varepsilon = \frac{2\pi}{L_s^{2/3}} \left(\frac{2\sigma_T^2}{3a} \right)^{3/2}. \quad (7)$$

The dissipation rate can be evaluated using aircraft measurements to assess the σ_T^2 estimate.

Each of the broadening mechanisms acts on all spectral components of the measured Doppler spectrum, which is characterized by the total spectrum width σ_D. The broadening terms are combined to provide a correction factor, δ in meters per second, by which the initial air motion estimate is increased in the direction of the arrow in Fig. 2 (positive is downward), given as

$$\delta = \sigma_D - \sqrt{\sigma_D^2 - (\sigma_T^2 + \sigma_S^2 + \sigma_B^2)}. \quad (8)$$

An analysis of the Doppler spectrum broadening terms based on retrievals in many cases during the MPACE time period indicates that the variance from these terms is, on average, 9% of the total spectrum variance; thus, the total variance is dominated by the size distribution effects. Indeed, the minimization of turbulent and shear effects on the Doppler spectrum was a primary objective in the design of the MMCR operational modes (Kollias et al. 2007). The typical correction (δ) to the vertical velocity estimate due to the broadening terms is 0.03 m s^{-1} (75% of the corrections were one radar velocity bin or less) compared to a typical total spectrum width of 0.6 m s^{-1}. Even the largest corrections were only two or three radar velocity bins. Thus, it is clear that the correction terms are relatively small compared to the actual spectrum width and the range of observed vertical velocities (see below).

In terms of the corrections themselves, the vertical shear of the vertical wind (48%) and the turbulence (37%) appear to be the largest contributors to the total correction terms. The beamwidth (8%) and horizontal shear of the vertical velocity (7%) terms are somewhat less important. These relative shear corrections are the case, even though the actual horizontal shear of the vertical velocity is greater than that in the vertical because of the relatively narrow beamwidth and long-range gate of the radar.

As long as the identification of small particles is dependable, the uncertainty of this retrieval is due to the correction terms and the ability to distinguish the Doppler spectrum signal from the noise. As a measure of the potential uncertainty due to broadening terms, the sensitivities of key inputs are examined. If the horizontal or vertical shear of the vertical winds is doubled, with all else held constant at typical values, δ would increase from its typical value of 0.030 to 0.035 and 0.077 m s^{-1}, respectively. If the amount of turbulence, characterized by the dissipation rate, were actually an order of magnitude larger, δ would increase to 0.073 m s^{-1}. All three of these extremes working in coordination result in $\delta = 0.13$ m s^{-1}, suggesting that even if the contributions to spectral broadening are grossly underestimated, the vertical velocity is still certain to within about 0.1 m s^{-1}. Additional uncertainty is introduced by the ability to distinguish the spectral signal from the noise. Based on the typical steep slope of the left spectral edge, the uncertainty caused by peak identification is also estimated to be no more than 0.1 m s^{-1}. Thus, the combined, worst case uncertainty is approximately 0.2 m s^{-1}.

4. An example

The case study from 1630 to 1800 UTC 9 October demonstrates the vertical motion and turbulent dissipation rate retrieval results. During this case, the layer of cloud liquid near the cloud top, within which the vertical air motions are derived, remains 600–700 m thick. The temporal evolution of vertical motions is seen in a vertical velocity time series at 1050 m (Fig. 3a), which reveals a periodic pattern with both up- and downdrafts. A mean updraft of about 0.5 m s^{-1} is observed, with variations of ± 2 m s^{-1} from the mean. Various scales of motion are evident in Fig. 3a, which are further revealed by a power spectrum analysis of the time series (Fig. 4).[1] Dominant scales of motion exist at frequencies from 0.002 to 0.04 s^{-1}. The nearly $-2/3$ slope at the high-frequency end of the spectrum suggests that in this case the turbulent inertial subrange may have been captured (e.g., Curry et al. 1988; Gultepe and Starr 1995). Turbulent dissipation rates for the case are highly variable with less vertical coherence than was observed for the air motions (Fig. 3c). The dissipation rates vary from about 10^{-5} to greater than 10^{-3} m^2 s^{-3}.

5. Verification of methods

Retrieved vertical air motion and turbulent dissipation rate are compared with aircraft measurements from the University of North Dakota Citation on 5, 6, 8, and 9 October in order to assess the retrieval quality. These flights were selected based on the availability of

[1] To compute the power spectrum, the time series in Fig. 3a was mean-centered, linearly detrended, and tapered with a Hanning window.

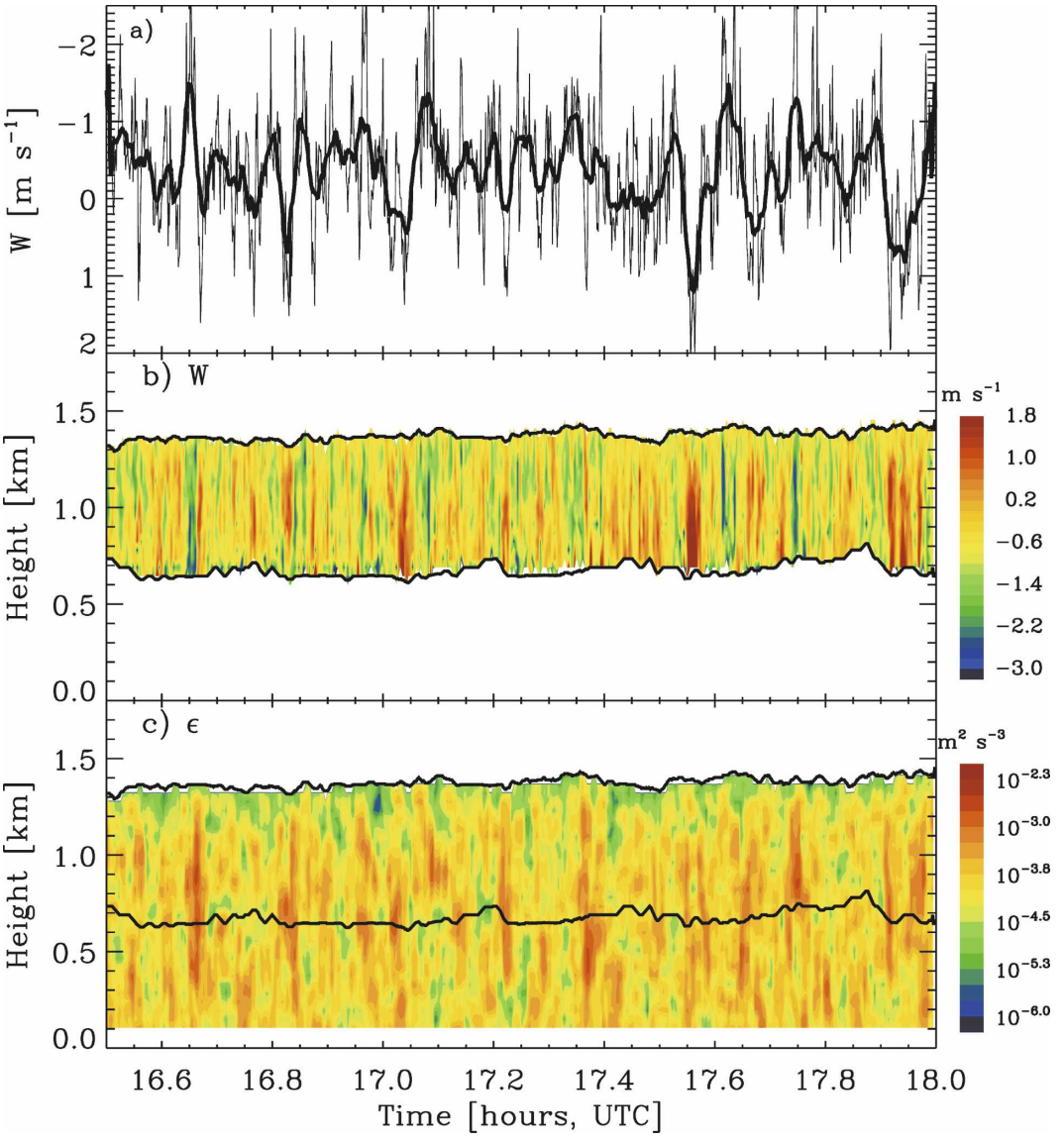

FIG. 3. Retrievals for the 9 Oct 2004 case of (a) vertical velocity at 1050 m, (b) vertical velocity, and (c) turbulent dissipation rate. In (b) and (c), the base and top of the cloud liquid layer are plotted. In (a), the data are plotted both in native resolution (~4 s) and with a 19-point (~80 s) smoothing window (thick line).

pertinent measurements and the proximity to the NSA site. However, because of flight patterns, the Citation was limited to distances of at least 2 km from the NSA site. Thus, statistical comparisons are made by sampling the ground-based results within time and height ranges that are bracketed by aircraft measurements within 20 km of the NSA site on a flight-by-flight basis (Fig. 5). The comparison dataset consists of ~50 000 ground-based retrieval points and ~5000 aircraft data points since the aircraft only samples at one height at a time and since some aircraft data were filtered out because of icing concerns. A statistical comparison is also made of aircraft spiral profiles near the site with ground-based retrievals that bracket the time period of the spirals (Fig. 6). Although this form of assessment does not specifically evaluate any single point in time and space (which is a difficult endeavor), it does allow for a more general comparison of the statistics and distributions of a given parameter over the same time and height ranges.

Since wind speed contributes to various components of the spectral broadening, the radiosonde-interpolated wind speed and direction are compared with aircraft measurements. Figure 5 shows that the wind directions

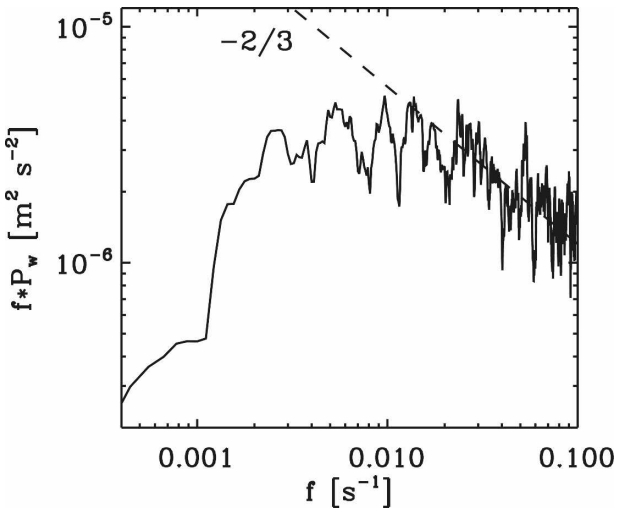

FIG. 4. Power spectrum of the time series of vertical velocity at 1050 m from Fig. 3a. A line of −2/3 slope has been included.

between these two datasets are nearly identically distributed from the east-northeast direction with a mean of ~12 m s^{-1}. The aircraft sampled a somewhat wider range of wind speeds than the periodic sounding measurements. The overall similarity of these measurements suggests that the interpolated radiosonde information used in the retrievals is both reasonably accurate and unbiased.

Eddy dissipation rates derived from the radar measurements are distributed similarly to those measured by the aircraft (Fig. 5d), albeit with a moderately larger number of small values. Nonetheless, the mean value retrieved by the radar is within ~5% of that observed by the aircraft in the comparison dataset. Vertical profile comparisons for three aircraft flights (Figs. 6b,d,f) provide a qualitative indication that the radar-derived dissipation rates are similar to those measured by the aircraft, although these too show a possible tendency for moderate underestimates by the ground-based retrievals in some cases. Overall, these comparisons suggest that the radar-based retrievals of turbulent spectral broadening are reasonable.

Both aircraft measurements and the radar-derived vertical velocities range from about −3 to 1.5 m s^{-1}, although the range of aircraft measurements is slightly larger (Fig. 5c). The distribution of radar-derived vertical velocities and the primary mode of the aircraft vertical velocity distribution appear to be offset by ~0.2 m s^{-1}. The aircraft observed a second mode at

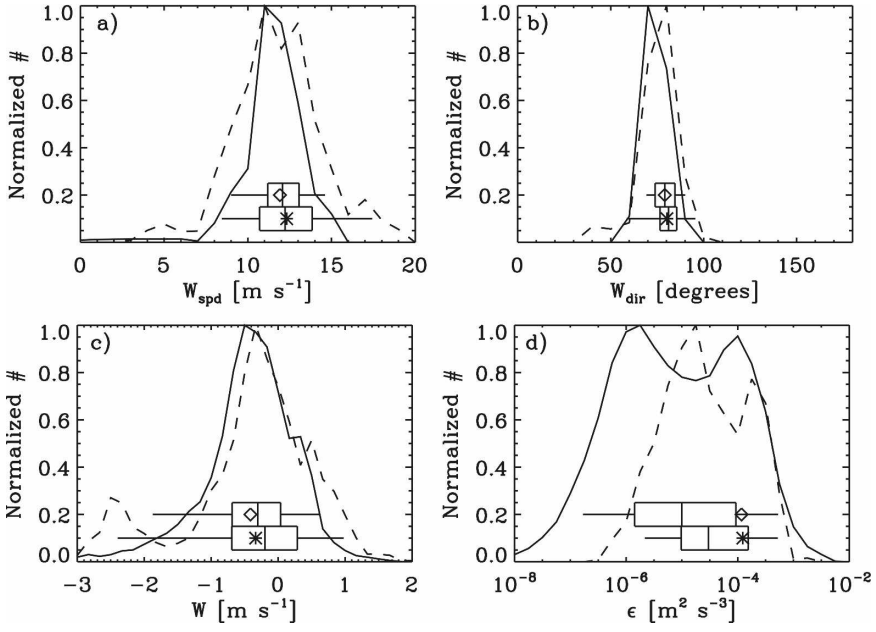

FIG. 5. Normalized distribution comparisons between aircraft measurements within 20 km of the NSA site (dashed and star) and measurements/retrievals from NSA instrumentation at coincident times (solid and diamond) during research aircraft flights on 5, 6, 8, 9, and 10 Oct of (a) wind speed, (b) wind direction, (c) vertical velocity, and (d) turbulent dissipation rate. Here, (a) and (b) utilize radiosonde measurements while (c) and (d) contain radar retrievals. Ground-based results used in this comparison dataset bracket the aircraft measurements in both time and space for each flight. Each distribution is normalized by its maximum value. The box-and-whisker plots provide the 5th, 25th, 50th, 75th, and 95th percentiles of the data and the symbol is the mean.

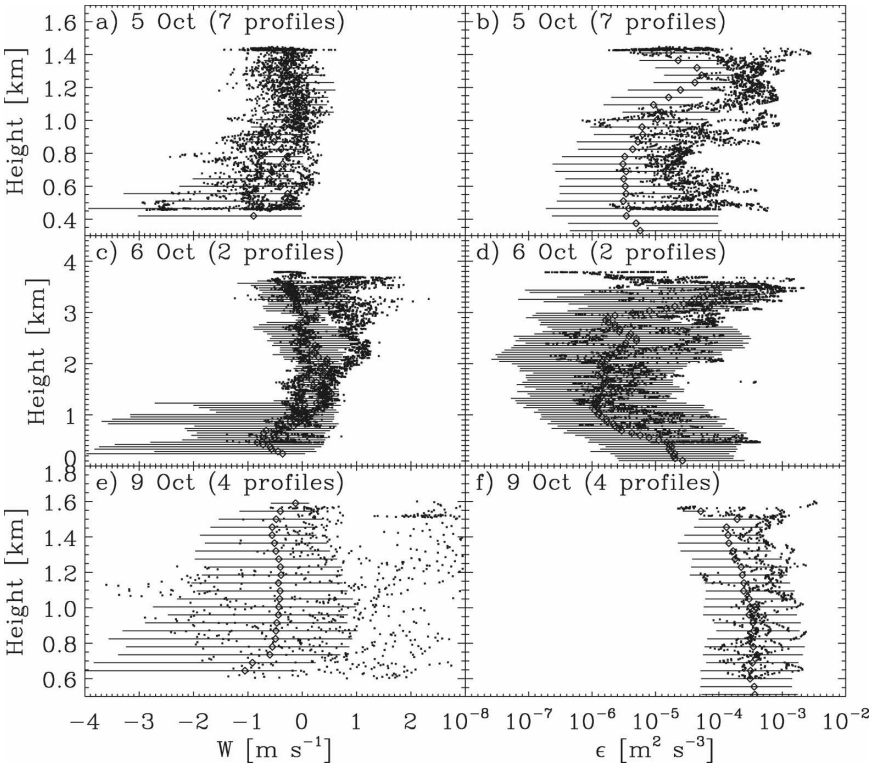

FIG. 6. Profile comparisons of (a), (c), (e) vertical velocity and (b), (d), (f) turbulent dissipation rate between aircraft measurements (dots) and radar retrievals for multiple aircraft profiles on three different days. The radar results are the mean (diamond) and range from the 5th to 95th percentile (line) for all data in a window that is ±5 min surrounding each aircraft profile.

-2.5 m s^{-1} that was not observed by the radar. Means and medians compare to within 0.1 m s^{-1}. Some vertical profile comparisons are quite good (Figs. 6a,c), while others show somewhat more scatter (Fig. 6e).

It is quite possible that observed differences are due to sampling distinct air masses and/or the uncertainties associated with computing W from each method. The error in aircraft vertical velocity is estimated to be 0.5 m s^{-1}, and although attempts were made to filter faulty data, some measurement errors due to aircraft icing may have gone undetected. Thus, the uncertainty of aircraft vertical wind estimates is significant here. In general, the radar W estimates should be fairly accurate and robust, as long as the identification of liquid droplets in a cloud volume is reliable, because the radar makes a direct measurement of radial (vertical) velocity of hydrometeors. Given the presence of liquid droplets, the assumption that they will have negligible fall speeds is sound. Thus, the net uncertainty of the W retrieval reduces to the uncertainty with which the spectral broadening terms can be determined and the spectral signal can be distinguished from the noise. As discussed above, uncertainties from these contributions are expected to be no more than 0.1 m s^{-1} each. In most cases, the comparisons between methods show agreement to within the expected uncertainties. The wide disparities during some portions of the 9 October comparison (Fig. 6e) suggest that different air masses may have been sampled at times.

6. Summary

A method for deriving vertical air motions in stratiform clouds containing liquid water droplets from cloud radar Doppler spectra is presented. The fundamental assumption made in the retrieval is that cloud liquid water droplets, which are on the order of 5–20 μm in size, have a negligible terminal fall speed and therefore act as tracers of vertical air motions. Included in the retrieval are corrections for spectral broadening terms that act to bias the vertical velocity estimate toward upward motion. The turbulent dissipation rate is a byproduct of this retrieval and is related to the turbulence spectral broadening correction term. For purposes of illustration, the retrieval method is demonstrated on measurements made by a 35-GHz cloud ra-

dar that is in operation at the ARM Climate Research Facility in Barrow, Alaska. This radar has been specifically configured to minimize spectral broadening effects due to turbulence and wind shear (Kollias et al. 2007). In addition to the cloud radar, supporting measurements from other active and passive sensors are used to identify the occurrence of cloud liquid and to provide an estimate of the horizontal wind speed for calculating some Doppler spectra broadening terms. The method may be applicable to similar radars and in other cloud conditions that contain small hydrometeors that can be assumed to trace vertical air motions.

Statistical comparisons of the radar-based retrieval results with research aircraft measurements of vertical velocity and turbulent dissipation rate suggest that the ground-based retrievals perform reasonably well. There appears to be a small ($\sim$0.2 m s^{-1}) bias between the radar retrievals and aircraft measurements of vertical velocity. Such a bias could be possible if the radar retrieval significantly underestimated the spectral broadening correction terms. A small underestimate is consistent with the abundance of small radar-derived turbulent dissipation rates compared to the aircraft measurements, which implies a possible underestimate of the turbulence broadening correction term in some cases. However, the magnitude of the differences in turbulence is not enough to fully account for the observed bias in vertical velocity. Thus, at least some portion of the bias may also be attributed to the relatively large uncertainty of aircraft vertical velocity measurements. Vertical profile comparisons of both parameters reveal that in many cases the radar-based retrievals and aircraft measurements reveal similar vertical structure.

Ground-based, remote sensing retrievals of vertical velocity, such as those demonstrated here, provide an important perspective for understanding cloud processes. For example, vertical velocity retrievals can be combined with estimates of cloud microphysical properties, which are also derived from radar and collocated instruments, to examine the associations between cloud dynamical and microphysical processes. In a companion study, Shupe et al. (2008) take advantage of this synergy to study the processes linking the cloud microphysical properties and vertical velocities in Arctic, autumn, mixed-phase clouds. That study develops a conceptual model that outlines the manner in which both cloud liquid and ice properties respond to vertical motions as part of a larger process that supports the extended lifetimes of Arctic mixed-phase clouds.

Acknowledgments. This research was supported by the Office of Science (BER), U.S. Department of Energy, Grant DE-FG02-05ER63965. Data were obtained from the ARM data archive. Thanks to the MPACE team and ARM for collecting the cloud datasets. Helpful discussions with Shelby Frisch and Chris Fairall are acknowledged.

REFERENCES

Babb, D. M., J. Verlinde, and B. W. Rust, 2000: The removal of turbulent broadening in radar Doppler spectra using linear inversion with double-sided constraints. *J. Atmos. Oceanic Technol.,* **17,** 1583–1595.

Bouniol, D., A. J. Illingworth, and R. J. Hogan, 2003: Deriving turbulent kinetic energy dissipation rate within clouds using ground based 94 GHz radar. Preprints, *31st Conf. on Radar Meteorology,* Seattle, WA, Amer. Meteor. Soc., 193–196. [Available online at http://ams.confex.com/ams/pdfpapers/63826.pdf.]

Curry, J. A., E. E. Ebert, and G. F. Herman, 1988: Mean and turbulent structure of the summertime Arctic cloudy boundary layer. *Quart. J. Roy. Meteor. Soc.,* **114,** 715–746.

Frisch, A. S., C. W. Fairall, and J. B. Snider, 1995: Measurements of stratus cloud and drizzle parameters in ASTEX with a K_α-band Doppler radar and a microwave radiometer. *J. Atmos. Sci.,* **52,** 2788–2799.

Gossard, E. E., 1994: Measurement of cloud droplet size spectra by Doppler radar. *J. Atmos. Oceanic Technol.,* **11,** 712–726.

——, and R. G. Strauch, 1983: *Radar Observations of Clear Air and Clouds*. Elsevier, 280 pp.

——, J. B. Snider, E. E. Clothiaux, B. Martner, J. S. Gibson, R. A. Kropfli, and A. S. Frisch, 1997: The potential of 8-mm radars for remotely sensing cloud drop size distributions. *J. Atmos. Oceanic Technol.,* **14,** 76–87.

Gultepe, I., and D. O'C. Starr, 1995: Dynamical structure and turbulence in cirrus clouds: Aircraft observations during FIRE. *J. Atmos. Sci.,* **52,** 4159–4182.

Heymsfield, A., 1975: Cirrus uncinus generating cells and the evolutions of cirriform clouds. Part II. The structure and circulations of the cirrus uncinus generating head. *J. Atmos. Sci.,* **32,** 809–819.

Hildebrand, P. H., and R. S. Sekhon, 1974: Objective determination of the noise level in Doppler spectra. *J. Appl. Meteor.,* **13,** 808–811.

Hogan, R. J., P. R. Field, A. J. Illingworth, R. J. Cotton, and T. W. Choularton, 2002: Properties of embedded convection in warm-frontal mixed-phase cloud from aircraft and polarimetric radar. *Quart. J. Roy. Meteor. Soc.,* **128,** 451–476.

Intrieri, J. M., M. D. Shupe, T. Uttal, and B. J. McCarty, 2002: An annual cycle of Arctic cloud characteristics observed by radar and lidar at SHEBA. *J. Geophys. Res.,* **107,** 8030, doi:10.1029/2000JC000423.

Kollias, P., and B. A. Albrecht, 2000: The turbulence structure in a continental stratocumulus cloud from millimeter-wavelength radar observations. *J. Atmos. Sci.,* **57,** 2417–2434.

——, ——, R. Lhermitte, and A. Savtchenko, 2001: Radar observations of updrafts, downdrafts, and turbulence in fair-weather cumuli. *J. Atmos. Sci.,* **58,** 1750–1766.

——, E. E. Clothiaux, M. A. Miller, E. P. Luke, K. L. Johnson, K. P. Moran, K. B. Widener, and B. A. Albrecht, 2007: The Atmospheric Radiation Measurement Program cloud profiling radars: Second-generation sampling strategies, process-

ing, and cloud data products. *J. Atmos. Oceanic Technol.,* **24,** 1199–1214.

Liljegren, J. C., E. E. Clothiaux, G. G. Mace, S. Kato, and X. Dong, 2001: A new retrieval for cloud liquid water path using a ground-based microwave radiometer and measurements of cloud temperature. *J. Geophys. Res.,* **106,** 14 485–14 500.

Lothon, M., D. H. Lenschow, D. Leon, and G. Vali, 2005: Turbulence measurements in marine stratocumulus with airborne Doppler radar. *Quart. J. Roy. Meteor. Soc.,* **131,** 2063–2080.

Moran, K. P., B. E. Martner, M. J. Post, R. A. Kropfli, D. C. Welsh, and K. B. Widener, 1998: An unattended cloud-profiling radar for use in climate research. *Bull. Amer. Meteor. Soc.,* **79,** 443–455.

O'Connor, E. J., R. J. Hogan, and A. J. Illingworth, 2005: Retrieving stratocumulus drizzle parameters using Doppler radar and lidar. *J. Appl. Meteor.,* **44,** 14–27.

Paluch, I. R., and D. H. Lenschow, 1991: Stratiform cloud formation in the marine boundary layer. *J. Atmos. Sci.,* **48,** 2141–2158.

Pinto, J. O., 1998: Autumnal mixed-phase cloudy boundary layers in the Arctic. *J. Atmos. Sci.,* **55,** 2016–2038.

Pruppacher, H. R., and J. D. Klett, 1978: *Microphysics of Clouds and Precipitation*. Reidel, 714 pp.

Rauber, R. M., and A. Tokay, 1991: An explanation for the existence of supercooled water at the top of cold clouds. *J. Atmos. Sci.,* **48,** 1005–1023.

Sassen, K., 1984: Deep orographic cloud structure and composition derived from comprehensive remote sensing measurements. *J. Climate Appl. Meteor.,* **23,** 568–582.

Shupe, M. D., 2007: A ground-based multiple remote-sensor cloud phase classifier. *Geophys. Res. Lett.,* **34,** L22809, doi:10.1029/2007GL031008.

——, P. Kollias, P. O. G. Persson, and G. M. McFarquhar, 2008: Vertical motions in Arctic mixed-phase stratiform clouds. *J. Atmos. Sci.,* **65,** 1304–1322.

Turner, D. D., S. A. Clough, J. C. Liljegren, E. E. Clothiaux, K. Cady-Pereira, and K. L. Gaustad, 2007: Retrieving liquid water path and precipitable water vapor from the Atmospheric Radiation Measurement (ARM) microwave radiometers. *IEEE Trans. Geosci. Remote Sens.,* **45,** 3680–3690.

Verlinde, J., and Coauthors, 2007: The Mixed-Phase Arctic Cloud Experiment. *Bull. Amer. Meteor. Soc.,* **88,** 205–221.

Zuidema, P., and Coauthors, 2005: An Arctic springtime mixed-phase cloudy boundary layer observed during SHEBA. *J. Atmos. Sci.,* **62,** 160–176.